

Development of a magnetic resonance imaging system for wet snow samples

Satoru ADACHI^{1*}, Satoru YAMAGUCHI², Toshihiro OZEKI³, and Katsumi KOSE⁴

1. Shinjo Cryospheric Environment Laboratory, Snow and Ice Research Center,

National Research Institute for Earth Science and Disaster Resilience,

Yamagata, Japan

* stradc@bosai.go.jp

2. Snow and Ice Research Center, National Research Institute for Earth Science

and Disaster Resilience, Niigata, Japan

3. Hokkaido University of Education, Sapporo, Japan

4. MRIsimulations Inc, Tokyo, Japan

(Received April 7, 2017; Revised manuscript accepted January 25, 2019)

Abstract

Understanding the behavior of water within snow cover, including its content, distribution, and movement, is essential for forecasting avalanches and for predicting the sliding of snow from the roofs of structures. We developed a high-resolution magnetic resonance imaging (MRI) system for non-destructive measurement of the distribution of water in snow cover. Our system is compact, uses a permanent magnet, and is designed for use in temperatures below 0 °C. To adapt the system to cold conditions, it was necessary to correct for inhomogeneities in the static magnetic field because a permanent magnet is strongly affected by the thermal conditions. We designed a single-layer shimming coil for this purpose. To prevent the wet snow sample from melting or freezing during scanning, we also developed a cooling system that uses a combination of liquid and air to maintain the sample at 0 °C. These improvements enabled non-destructive visualization of the water distribution in a wet snow sample, with high resolution. We therefore propose our MRI system as a powerful tool that can contribute to the understanding of wet snow physics.

Key word: Wet snow, Magnetic resonance imaging, Liquid water content, Inhomogeneity of water content, Non-destructive visualization

1. Introduction

Snow cover, which comprises ice and air, and possibly liquid water, is a complex porous medium. A major difference between snow cover and other porous media is that its characteristics change rapidly under wet conditions, as water significantly affects the size, shape, and inter-particle connections of the constituent ice grains. An understanding of the behavior of water in snow cover (specifically its distribution and movement) is critical for forecasting disasters such as avalanches and wet snow sliding from roofs.

Previous studies of wet snow cover have been limited to macroscopic studies of the behavior of water within it (*e.g.*, Avanzi *et al.*, 2016; Katsushima *et al.*, 2013; Yamaguchi *et al.*, 2010, 2012), and therefore they could not discuss in detail the relationship between the microstructure of the snow cover and its water content distribution. Further, it was impossible to continuously monitor the changes in a sample under wet conditions because it was necessary to destroy the sample to measure the water distribution. To advance the understanding of the physical characteristics of wet snow cover in detail requires a non-destructive, high-resolution method for measuring the water distribution.

Magnetic resonance (MR) imaging (MRI) can image nuclear MR (NMR) signals from protons in a liquid, and is commonly used in medical applications to image tissues such

as the brain and tendons, which have a high water content. If MRI is applied to snow, it is not possible to image the snow particles directly, because they are composed of solid water (ice). However, MRI could be used to image the distribution of liquid water in wet snow cover.

The first attempt to use MRI to investigate the structure of snow cover was made by Ozeki *et al.* (2003), who used a superconducting magnet in a laboratory at room temperature, along with a cold chamber to cool the snow sample (alone) to below 0 °C. They filled gaps in the snow with dodecane (C₁₂H₂₆, melting point -12 °C) and obtained NMR images of the dodecane. In the resulting 3D MR images, dodecane appeared strongly hyperintense compared with the snow particles, and the images were then inverted to display the snow as bright. The study was an innovative attempt to apply MRI to the study of snow and ice. However, as the temperature inside a superconducting magnet cannot be measured, detailed temperature control is impossible; therefore, MRI using superconducting magnet is not applicable to wet snow samples, which need to be kept at 0 °C to prevent the samples from melting or freezing. Strict temperature management of snow samples requires the MRI instrument itself to be in a cold environment. However, superconducting magnets are too large and heavy for installation in a general cold room, and they require cooling with liquid

nitrogen and liquid helium, which pose a risk of asphyxiation if they leak. Therefore, we concluded that a superconducting magnet system is not suitable for the imaging of wet snow.

We used a compact MRI system for imaging wet snow because this system employs a small permanent magnet and a small console (Haishi *et al.*, 2001), and has none of the problems associated with a superconducting magnet. In the first system that we developed, a permanent 1.0 T magnet was located in a cold-room laboratory at $-5\text{ }^{\circ}\text{C}$ (Adachi *et al.*, 2007, 2009). Although this system had a small field of view (a spherical volume of diameter $\sim 30\text{ mm}$), it could obtain a 3D dataset of pores and snow particles in dry snow cover, using dodecane to fill the pores in the same manner as that employed by Ozeki *et al.* (2003). The system was also used to image a brine channel in sea-spray ice, with spatial resolution of $(123\text{ }\mu\text{m})^3$ (Adachi *et al.*, 2006, Ozeki *et al.*, 2007). These results were the first to demonstrate the potential of the permanent-magnet MRI system to obtain images of the same quality as those obtained by a superconducting system.

However, our first system faced problems when measuring the detailed 3D distribution of water in a snow sample; namely, the diameter of the case holding the sample (24 mm) was too small for imaging wet snow because the walls could affect the behavior of the water inside it. For this reason, we designed a new MRI system capable of performing

detailed investigation of the 3D distribution of water inside a snow sample. This work introduces the new system, which is more suitable for wet snow than is the previous system.

2. New MRI system

The new MRI system developed in this study comprises seven parts (Fig. 1, Table 1): a permanent 0.21 T magnet (Fig. 2), a gradient coil (G coil) set (Fig. 3), a single layer shimming coils (SLS coil) (Fig. 4) (Tamada *et al.*, 2011), a radio frequency (RF) probe (Fig. 5), a thermostatic bath, a cooling fan, and an MRI console (Fig. 6). A large, strong (0.21 T) magnetic field exists in the 0.25 m gap between the poles of the U-shaped, magnetized neodymium permanent magnet. The three G coils (one for each orthogonal axis) provide 3D position information. The RF probe transmits the RF signal to the sample and receives the resulting signal from the sample. In addition, it is possible to set up a cylindrical sample holder with 0.11 m in diameter. The MRI console consists of a PC, a power supply for the gradient/shimming coil sets, and a transceiver for the NMR signal. The components of the MRI system in the cold room (0 °C) and those outside it at room temperature were connected by cables through ducts to the cold room.

Fig. 1(半

Table 1
(全幅)

Fig. 2(全

Fig. 3(全

Fig. 4(全

Fig. 5(全

Fig. 6(半

2.1. Imaging method for wet snow

As described in the next section, the inhomogeneity of the static magnet field of the permanent magnet has been corrected by using the SLS coil, however some inhomogeneity still remains. To acquire MR images of wet snow under the condition of an inhomogeneous magnetic field, we first selected a spin echo (SE) sequence (Hahn, 1950) because SE does not use a magnetic field to generate NMR signal (Bernstein *et al.*, 2004). The MR image matrix of the SE sequence was $128 \text{ (read)} \times 128 \times 128$ pixels with spatial resolution of 1 voxel representing 1 mm, repetition time (TR) 3000 ms, and echo time (TE) 100 ms. Because it took ~14 h to capture one MR image, which is much longer than timescales of changes in the structure of the wet snow and of movement of the water in it, the technique was not suitable for imaging wet snow. To reduce the imaging time, we progressed to using fast SE (FSE) and driven equilibrium SE (DESE) sequences (Iita *et al.*, 2007). FSE and DESE sequences both employ an excitation pulse, but the former involves eight refocusing pulses (imaging time 100 min), while the latter uses refocusing pulses with flip angles of 90° , 180° , and -90° (imaging time ~30 min). Although DESE achieved the quickest imaging, the heat generated by the G coils was greater with this sequence than the others. For this reason, DESE was used

only to take a rough image of the distribution of water in the snow cover sample, and FSE was used to acquire the images used for detailed analyses of the wet snow.

2.2. Correction of inhomogeneity in the magnetic field

In general, the magnetic field of a permanent magnet is optimized at room temperature, and changes with alterations in temperature. Although the homogeneity of the field of our permanent magnet was 25 ppm (part per million) over a 0.15 m diameter spherical volume within the gap at room temperature, the homogeneity cannot be ensured at cold room (0 °C). To correct for inhomogeneity, we installed an SLS coil inside the G coil set, between the poles of the permanent magnet (Terada *et al.*, 2013) (Fig. 2).

The design of the SLS coil was determined as follows. The magnetic field distribution was measured using an inhomogeneous MR image of a three-dimensional (3D) lattice phantom (Fig. 7). The superposition of circular currents, which can produce a current density to correct the inhomogeneity of the field at each position in the multi-square lattice, was determined by the method of Juchem *et al.* (2010, 2011). The stream function method (Tamada *et al.*, 2011) was used to calculate the number of windings necessary to produce the required circular current. Based on the resulting winding pattern (Fig. 4(a)), an SLS coil

Fig. 7 (全幅)

comprising one copper wire (diameter: 1 mm) was wound on the fiber-reinforced plastic board (Fig. 4(b)).

Figure 8 shows MR images of the 3D lattice sample. The uncorrected images show distortions caused by inhomogeneity in the magnetic field of the permanent magnet that was caused by thermal change; *i.e.*, distortion in the lattice pattern in Fig. 8(a). In addition, the

Fig. 8(全)

clear lattice pattern seen on the left of Fig. 8(b) is degraded on the right side by a large area of shadow. The lack of such distortions in Fig. 8(c) and (d) indicates an improvement in the homogeneity of the static magnet field. To evaluate the homogeneity of the static magnetic

field before (Fig. 9(a)) and after (Fig. 9(b)) distortion correction with the SLS coil, we

Fig. 9(全幅)

calculated and imaged the static magnet field under each condition. In the field of MRI/NMR, the homogeneity of a static magnetic field is expressed (in units of ppm) as the difference from the standard frequency, according to the magnetic field. In a uniform static magnetic field, the values over the whole space are close to 0 ppm. When no current was applied to the SLS coil, the root mean square (RMS) homogeneity of the static magnetic field was 3.2 ppm in the measurement area. In contrast, when a current of 450 mA was applied to the SLS coil, the RMS homogeneity of the static magnetic field became 1.3 ppm, an improvement of about 2.5 times.

2.3. Cooling system for maintaining constant temperature in the MRI system

There were two problems associated with maintaining the temperature of the wet snow sample at 0 °C in the permanent magnet: warming due to the intermittent current flow in the G coils and the continuous current flow in the SLS coil; and fluctuation in the temperature (approximately ± 2 °C) of the cold room itself, despite it being set at 0 °C. We proposed two solutions to address these problems. The first was to add space between the sample space and the heat sources. In general, G coils are fixed tightly to the permanent magnet so that vibrations caused by the electromagnetic force do not dislodge them; however, we added a 30 mm clearance between the permanent magnet and the G coils using a jig (Fig. 2) to protect the sample against heat transfer from the G coils. We also left a 5 mm clearance between the RF probe and the coils to protect the sample against heat transfer from the G coils. Because our experimental condition did not cause a great amount of vibration in the G coils, adding the space did not have an adverse effect on image quality. Our second improvement was to modify the system to maintain a constant sample temperature of 0 °C by incorporating a silicone tube wound around the RF bobbin (Fig. 5). Antifreeze liquid at 0 °C was then circulated through the silicon tube using a thermostatic bath. Although the antifreeze liquid in

the silicon tube could be visualized outside the snow sample, it did not affect the region of interest in the MR image. We employed both of these methods when imaging the wet snow.

To evaluate the ability of the cooling system to maintain the sample at a constant temperature, we measured the temperature during DESE imaging, with the cold room set at 0 °C. A temperature sensor (HOBO TMC 20-HD) was set inside the RF bobbin to measure the temperature of the sample, and similar sensors were also set on the surface of the G coils and immediately above the magnet. For all sensors, temperature was measured at 30 s intervals. The cold room temperature periodically varied from about -3 to 1 °C, which was related to the intermittent operation of its cooling system. When the cooling system was disabled, the temperature of the G coils rose above 4 °C (Fig. 10(a)) and fluctuated within 0.5 °C during operation of the cooling system (Fig. 10(b)). The temperatures of the samples and the G coils rose to 2 °C after 60 min without the cooling system (Fig. 10(a)), whereas averaged over 60 min, the sample was maintained at 0 °C using the cooling system (Fig. 10(b)). These results demonstrate the effectiveness of our cooling system.

Fig. 10(半

3. MR image of wet snow

Water retention curves (WRCs), which show the relationship between volumetric water content and suction, are fundamental for characterizing hydraulic properties. The WRC of snow therefore has been investigated to understand the movement of water within it (*e.g.*, Yamaguchi *et al.*, 2010). To validate the performance of MRI for the study of wet snow, we imaged the WRC of snow. The snow sample was sieved to select particle diameters of 1.7 to 2.0 mm and then packed in a sample holder of diameter 80 mm and height 100 mm. Water was introduced from the bottom of the sample holder and then left for about 30 min, during which time it rose into the sample under capillary force of the snow structure, to reach a steady state. Figure 11 shows the vertical profile of the sample after reaching steady state, in an MR image acquired with DESE (8-bit [256 level] grayscale image, 128×128 pixels, 1 mm spatial resolution). The amount of water in the sample is indicated by the grayscale value on the figure, with a brighter shade indicating more water. Above the hydraulic head (marked by the dashed line in Fig. 11), the lack of signal from the snow particles indicates a lack of liquid water in this area. Figure 12 shows the distribution of the mean grayscale value with height from the free water surface calculated from Fig. 11. Each average considered the levels of 80 pixels (horizontal width 80 mm, vertical width 1 mm). The mean gray values are highest between the free water surface and height of 20 mm, decrease sharply from 21 to 35 mm, and

Fig. 11(半幅)

Fig. 12(半幅)

remain at 0 after 36 mm. The trend of the mean grayscale value distribution is similar to that of the WRC measured by Yamaguchi *et al.* (2010). In addition, the area of rapid decrease in mean grayscale value corresponds to the area of the hydraulic head (Fig. 11) and is not at a constant height, implying inconsistency in the microstructure (namely the air gap distribution) of the sample. This information cannot be obtained using conventional research methods. Therefore, the investigation of the WCR of snow using our MRI method should provide new knowledge regarding the relationship between the microstructure of snow and its water distribution.

4. Conclusion

We developed a new MRI system based on a compact MRI system with a permanent magnet to measure the water distribution in wet snow cover non-destructively and at high resolution. To use the system at low temperature, it was necessary to correct inhomogeneity in the permanent magnet's magnetic field that results from change in the thermal conditions. The SLS coil designed for this purpose improved the uniformity of the static magnetic field and enabled the acquisition of images free of distortions. We also developed a cooling system, using a combination of liquid cooling and air cooling, to

maintain the temperature of the wet snow sample at 0 °C during imaging and thus prevent melting or freezing of the sample. The implementation of these improvements in our system enabled non-destructive and high-resolution visualization of the water distribution in a wet snow sample. Analysis of the MR image of the WRC of wet snow revealed a similar distribution of brightness to the measured water content distribution along the WRC. If the method of using MRI to measure water content volumetrically in bone (Kose *et al.*, 2004) can be applied to wet snow, we can derive from MR image of wet snow its quantitative water content distribution. Such information should be useful for understanding the behavior of water in snow cover. Although we need the verification of this method based on comparison between water content calculated from MR image and water content measured with traditional method such as dielectric constant (Denoth *et al.*, 1984) and calorimeter (Kawashima *et al.*, 1998), we think that our new system is a powerful tool which is applied to advance the understanding of wet snow physics.

Acknowledgment

We wish to thank Dr. Tomoyuki Haishi at MRTechnology, Inc., Dr. Kuniyasu Ogawa at Keio University, Dr. Kouichi Nishimura at Nagoya University and Dr. Kenji Kosugi

at Snow and Ice research center, NIED for their helpful discussions. We are grateful to Dr. Daiki Tamada at the University of Yamanashi for help with the numerical simulations and to Shunichi Nakatsubo at the Japan Aerospace Exploration Agency for assisting with the fabrication of a 3D lattice phantom.

References

Adachi, S., Ozeki, T. and Haishi, T. (2006): Imaging of drainage channels in sea spray icing by compact MRI system (in Japanese). *Cold Region Technology collection of papers*, **22**, 86–89.

Adachi, S., Ozeki, T., Kose, K., Handa, S. and Haishi, T. (2007): Development of MRI sequence for visualization of snow structures - 3D driven equilibrium spin-echo sequence and dual scan – (in Japanese). *Cold Region Technology collection of papers*, **23**, 140–144.

Adachi, S., Ozeki, T., Shigeki, R., Handa, S., Kose, K., Haishi, T. and Aoki, M. (2009): Development of a compact magnetic resonance imaging system for a cold room. *Rev. Sci. Instrum.*, **80**, 054701, 1–4, doi: 10.1063/1.3129362.

Adachi, S., Yamaguchi, S., Ozeki, T. and Kose, K. (2017): Current status of application of cryospheric MRI to wet snow studies (in Japanese with English Abstract). *J. Jpn. Soc. Snow and Ice (Seppyō)*, **79**, 6, 497–509.

Avanzi, F., Hirashima, H., Yamaguchi, S., Katsushima, T. and De Michele, C.

(2016): Observations of capillary barriers and preferential flow in layered snow during cold laboratory experiments. *The Cryosphere*, **10**, 2013–2026, doi: 10.5194/tc-10-2013-2016.

Bernstein, M., King, K. and Zhou, X. (2004): *Handbook of MRI Pulse Sequences*, 1st ed.

Academic Press. ISBN: 9780120928613.

Denoth, A., Foglar, A., Weiland, P., Mätzler, C., Aebischer, H., Tiuri, M. and Sihvola, A.

(1984): A comparative study of instruments for measuring the liquid water content of snow. *J. Appl. Phys.*, **56**, 2154-2160, doi: 10.1063/1.334215.

Hahn, E. L. (1950): Spin echoes. *Phys. Rev.*, **80**, 580–594, doi: 10.1103/PhysRev.80.580.

Haishi, T., Uematsu, T., Matsuda, Y. and Kose, K. (2001): Development of a 1.0 T MR microscope using a Nd-Fe-B permanent magnet. *Magn. Reson. Imaging*, **19**, 875–880.

Iita, N., Handa, S., Tomiha, S. and Kose, K. (2007): Development of a compact MRI system for measuring the trabecular bone microstructure of the finger. *Magn. Reson. Med.*, **57**, 272–277, doi: 10.1002/mrm.21130.

Juchem, C., Nixon, T., McIntyre, S., Rothman, D. and Graaf, R. (2010): Magnetic field modeling with a set of individual localized coils. *J. Magn. Reson.* **204**, 281–289, doi: 10.1016/j.jmr.2010.03.008.

Juchem, C., Nixon, T., McIntyre, S., Boer, V., Rothman, D. and Graaf, R. (2011): Dynamic multi-coil shimming of the human brain at 7 T. *J. Magn. Reson.*, **212**, 280–288, doi: 10.1016/j.jmr.2011.07.005.

Katsushima, T., Yamaguchi, S., Kumakura, T. and Sato, A. (2013): Experimental analysis of preferential flow in dry snowpack. *Cold. Reg. Sci. Technol.*, **85**, 206–216, doi: 10.1016/j.coldregions.2012.09.012.

Kawashima, K., Endo, T. and Takeuchi, Y. (1988): A portable calorimeter for measuring liquid-water content of wet snow. *Ann. Glaciol.*, **26**, 103-106, doi: 10.3189/1998AoG26-1-103-106.

Kose, K., Matsuda, Y., Kurimoto, T., Hashimoto, S., Yamazaki, Y., Haishi, T., Utsuzawa, S., Yoshida, H., Okada, S., Aoki, M. and Tsuzaki, T. (2004): Development of a compact MRI system for trabecular bone volume fraction measurements. *Magn. Reson. Med.*, **52**, 440–444, doi: 10.1002/mrm.20135

Ozeki, T., Kose, K., Haishi, T., Hashimoto, S., Nakatsubo, S. and Nishimura, K. (2003): Three-dimensional snow images by MR microscopy. *Magn. Reson. Imaging*, **21**, 351–354.

Ozeki, T., Yamamoto, R., Adachi, S. and Kose, K. (2007): NMR imaging of sea spray icing and ice adhesion tests of pliable polymer sheets for deicing. *Proceedings of 12th International Workshop on Atmospheric Icing of Structures*, **12**, 6-6.

Tamada, D., Terada, Y. and Kose, K. (2011): Design and evaluation of a planar single-channel shim coil for permanent magnetic resonance imaging magnet. *Appl. Physics Express*, **4**, 066702, 1–3, doi: 10.1143/APEX.4.066702

Terada, Y., Ishi, K., Tamada, D. and Kose, K. (2013): Power optimization of a planar single-channel shim coil for permanent magnet circuit. *Appl. Physics Express*, **6**, 026701, 1–3, doi: 10.7567/APEX.6.026701.

Yamaguchi, S., Katsushima, T., Sato, A. and Kumakura, T. (2010): Water retention curve of snow with different grain sizes. *Cold. Reg. Sci. Technol.*, **64**, 87–93, doi: 10.1016/j.coldregions.2010.05.008

Yamaguchi, S., Watanabe, K., Katsushima, T., Sato, A. and Kumakura, T. (2012): Dependence of the water retention curve of snow on snow characteristics. *Ann. Glaciol.*, **53**, 6–12, doi:

10.3189/2012AoG61A001

Figure and Table captions:

Table 1: Elements of the MRI system

Fig. 1. Overview of the MR system for imaging wet snow. The permanent magnet, radiofrequency probe and sample are installed in a cold room. The MRI console is installed in a laboratory at room temperature. The thermostatic bath and fan are part of the cooling system.

Fig. 2. Mounting positions of the gradient coil set and pair of single layer shimming coils on the 0.21 T permanent magnet. (a) Diagram. (b) Photograph.

Fig. 3. Appearance of the gradient (G) coil sets. Each pair (Gx pair, Gy pair, Gz pair) is installed opposite each other inside the magnet.

Fig. 4. Appearance of the single layer shimming (SLS) coil. The paired SLS coils are installed opposite each other in the magnet. (a) Contour lines show the winding pattern. (b) Photograph.

Fig. 5. (a) Diagram and (b) photograph of the RF probe. A solenoid coil is wrapped around a bobbin, and silicon tube is wrapped so as to cover them.

Fig. 6. Appearance of the MRI console

The console consists of a PC, power supply for the G and SLS coils, amplifier, and transceiver for the NMR signal.

Fig. 7. Schematic of 3D lattice phantom

The phantom comprises 13 acrylic discs (thickness 10 mm, diameter 104 mm) with square trenches (cut-outs, $8 \times 8 \text{ mm}^2$ at 4 mm intervals) stacked in a cylindrical container (length 170 mm, inner and outer diameters of 104 and 110 mm, respectively) filled with baby oil (main ingredient: mineral oil) (a) horizontal and (b) vertical 2D section images.

Fig. 8. MR image of the 3D lattice sample (based on Adachi et al., 2017). (a) Vertical and (b) horizontal 2D section MR images before correction. The corresponding (c) vertical and (d) horizontal 2D section MR images after correction. The images in (b) and (d) are taken at the

white dashed line shown on (a) and (c), respectively.

Fig. 9. Correction effect of the SLS coil on the homogeneity of the static magnetic field.

Shimming coil current values were (a) 0 A (RMS = 3.2 ppm) and (b) 450 mA (RMS = 1.3 ppm).

Fig. 10. Temperature changes during MR imaging (a) without and (b) with a cooling system.

Fig. 11. Vertical MR image (2D section) of a wet snow sample. The broken line indicates the hydraulic head.

Fig. 12. Variation with height from the free water surface of the mean grayscale value (related to water content) in the MR image of wet snow in Fig. 11. A higher value indicates a greater liquid water content.

Table 1.

Device Configuration	Location	Figure number
Permanent magnet (0.21 T)	Cold room	Fig. 2
Gradient coil set	Cold room	Fig. 3
Single layer shimming coil	Cold room	Fig. 4
Radio frequency probe	Cold room	Fig. 5
Thermostatic bath	Cold room	–
Cooling fan	Cold room	–
MRI console /Personal computer /Transceiver /Gradient coil set power supply /Amplifier /Single layer shimming coil power supply	Laboratory	Fig.6

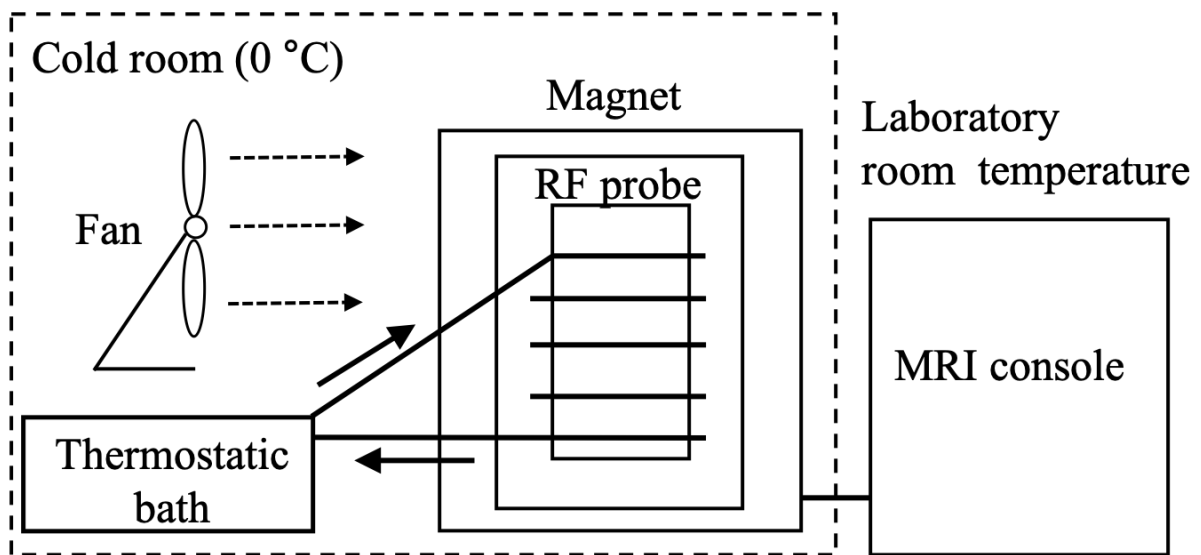


Figure 1.

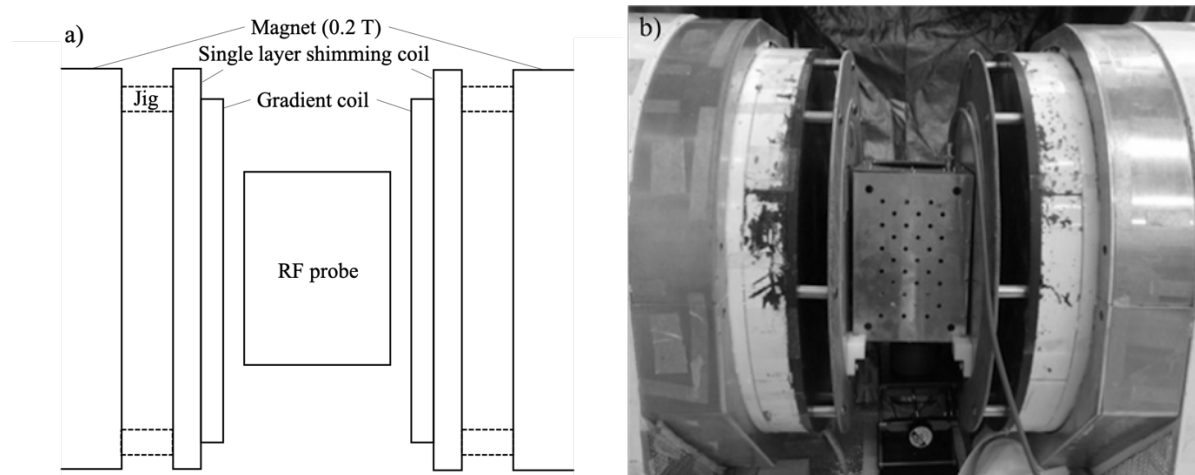


Figure 2.

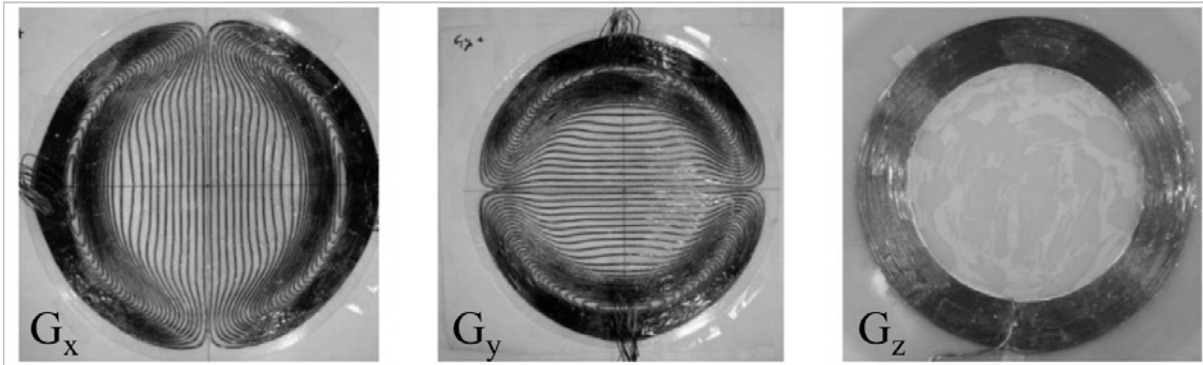


Figure 3.

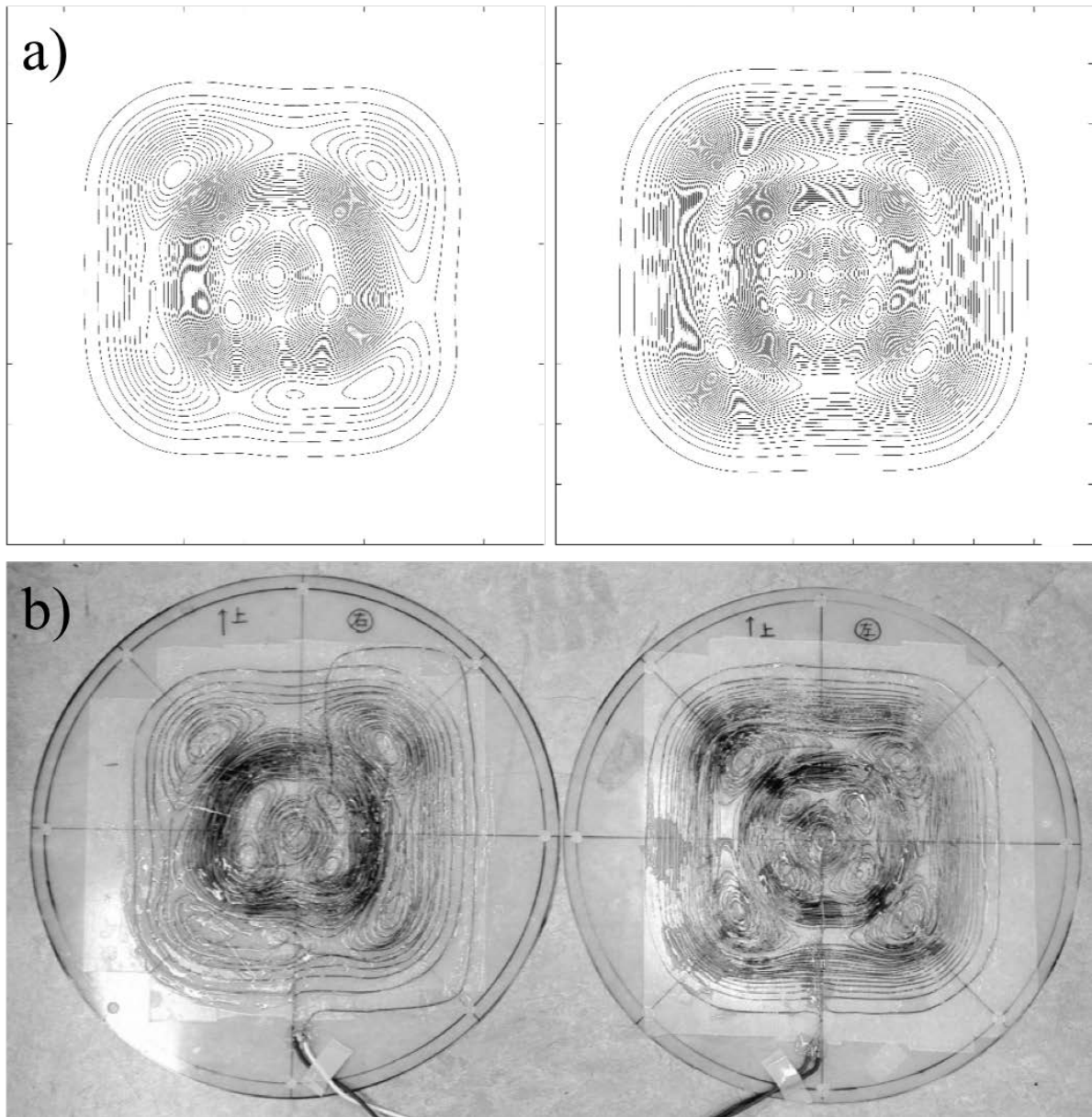


Figure 4.

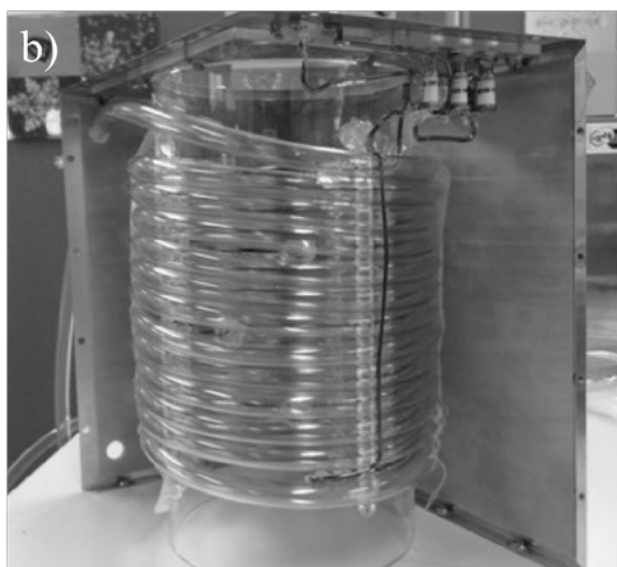
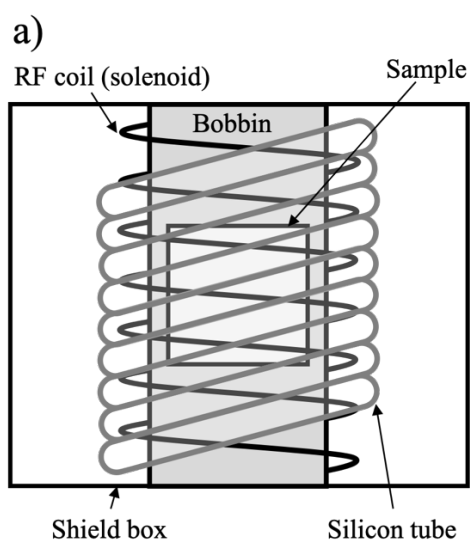


Figure 5.



Figure 6.

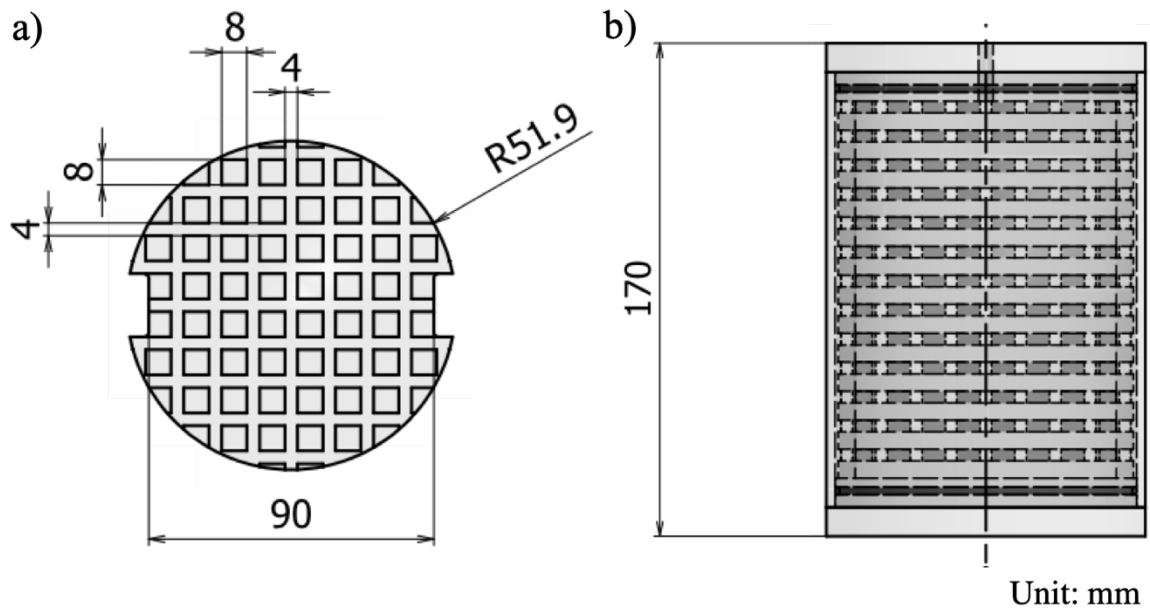


Figure 7.

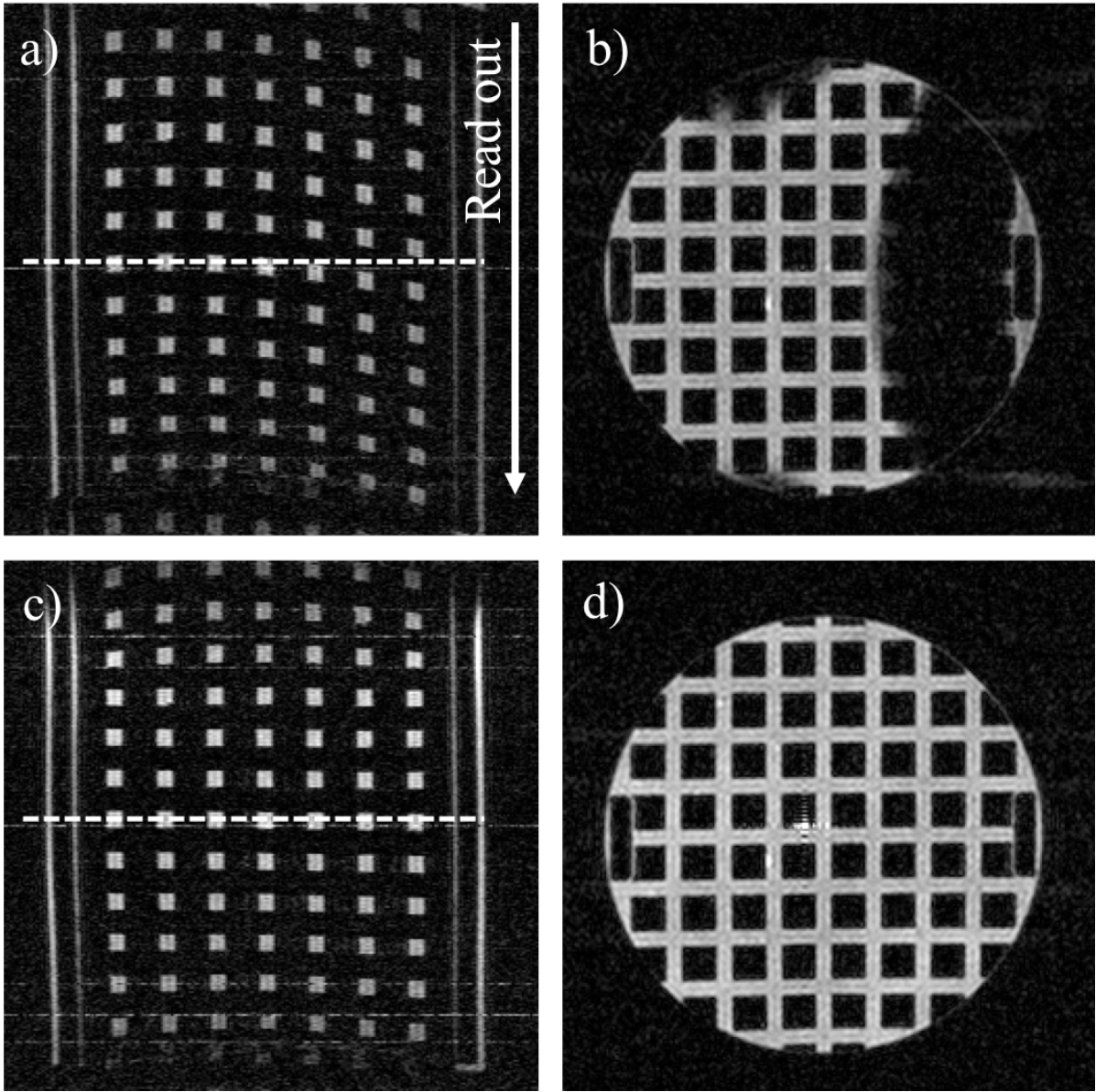


Figure 8.

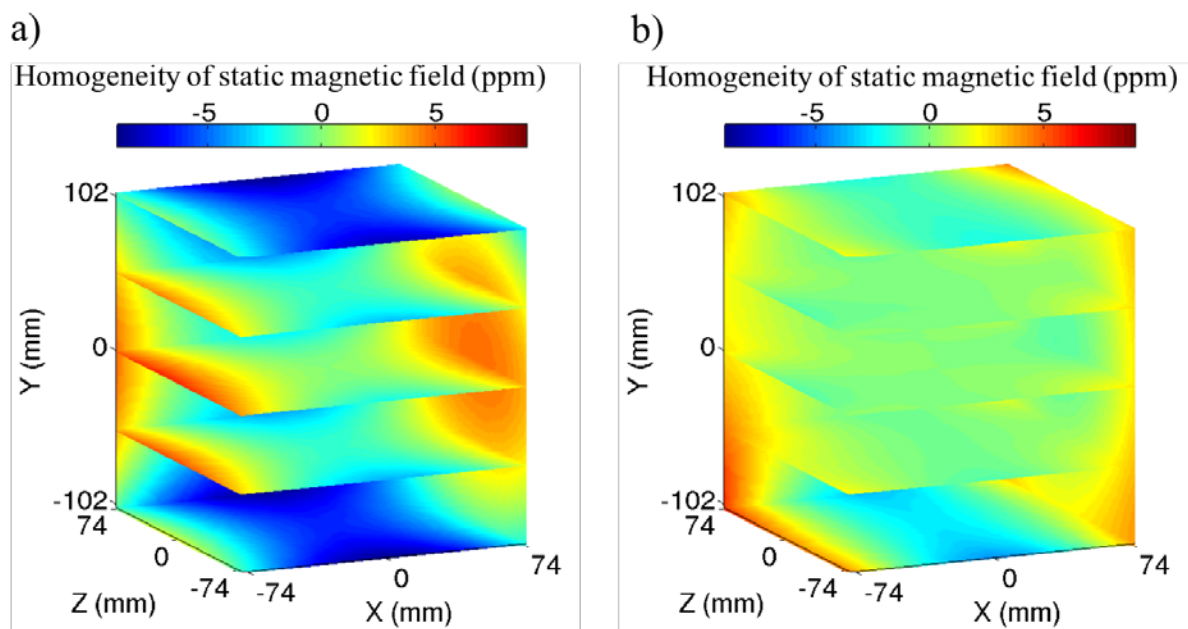


Figure 9.

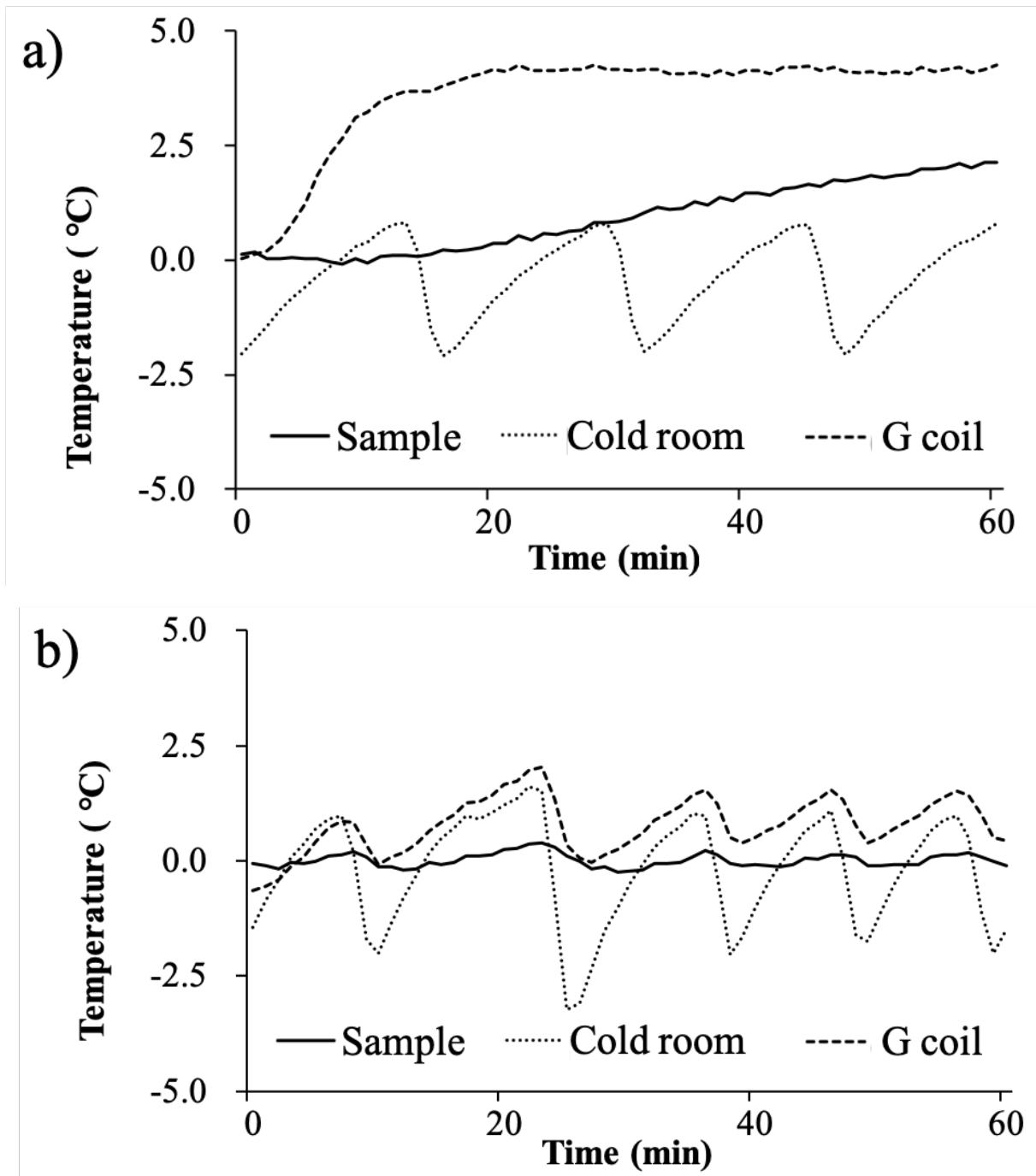


Figure 10.

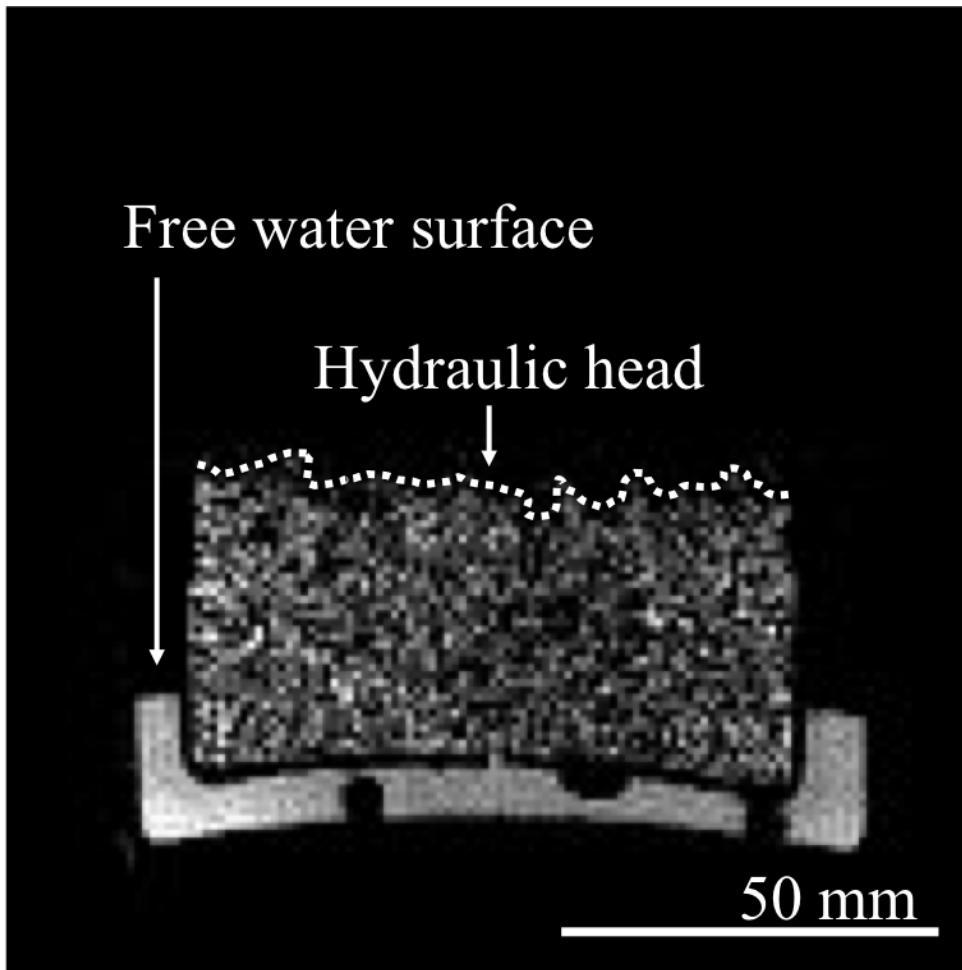


Figure 11.

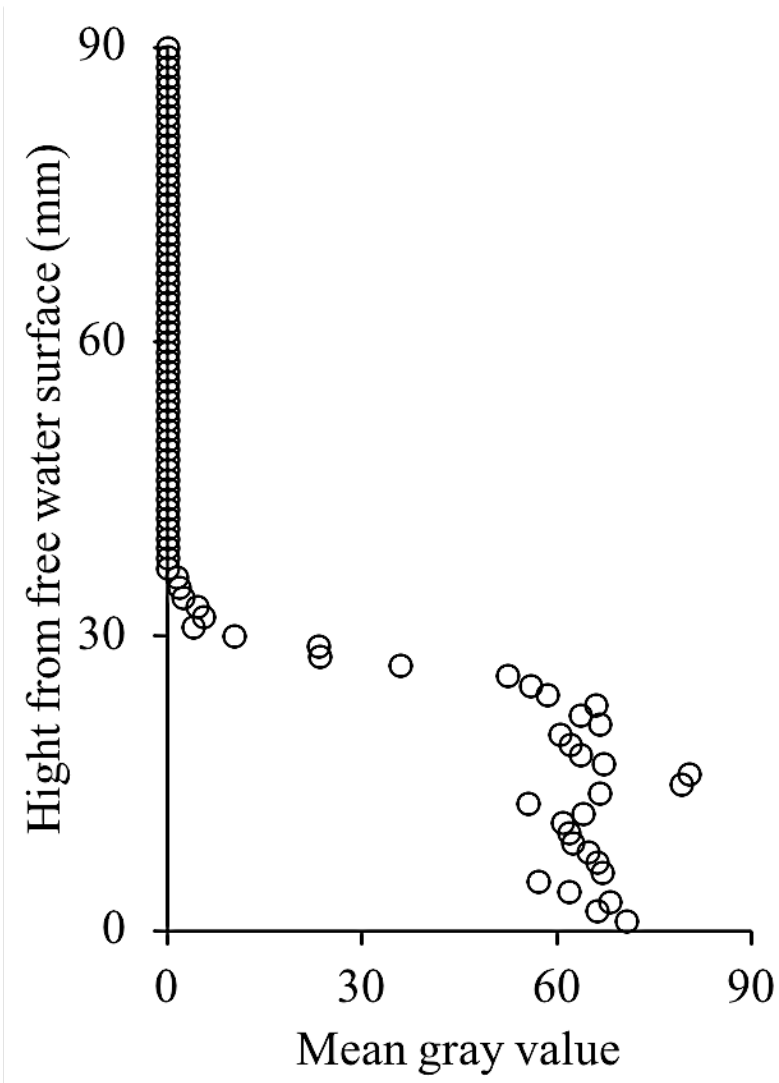


Figure 12.